Avalanche shapes in the fiber bundle model

Narendra Kumar Bodaballa and Soumyajyoti Biswas*
Department of Physics, SRM University AP, Amaravati 522240, Andhra Pradesh, India

Parongama Sen†
Department of Physics, University of Calcutta, Kolkata 700 009, India

(Received 11 October 2023; revised 11 April 2024; accepted 14 June 2024; published 19 July 2024)

We study the temporal evolution of avalanches in the fiber bundle model of disordered solids, when the model is gradually driven towards the critical breakdown point. We use two types of loading protocols: (i) quasistatic loading and (ii) loading by a discrete amount. In the quasistatic loading, where the load is increased by the minimum amount needed to initiate an avalanche, the temporal shapes of avalanches are asymmetric away from the critical point and become symmetric as the critical point is approached. A measure of asymmetry (A) follows a universal form $A \sim (\sigma - \sigma_c)^{\theta}$, with $\theta \approx 0.25$, where σ is the load per fiber and σ_c is the critical load per fiber. This behavior is independent of the disorder present in the system in terms of the individual failure threshold values. Thus it is possible to use this asymmetry measure as a precursor to imminent failure. For the case of discrete loading, the load is always increased by a fixed amount. The dynamics of the model in this case can be solved in the mean field limit. It shows that the avalanche shapes always remain asymmetric. We also present a variable range load sharing version of this case, where the results remain qualitatively similar.

DOI: 10.1103/PhysRevE.110.014129

I. INTRODUCTION

Intermittent avalanche dynamics are seen in a myriad of systems, including invasion of fluid in a porous media, moving domain walls in impure magnetic materials, compressed rocks prior to breakdown, and sliding tectonic plates causing earthquakes. The statistical nature of these avalanches, particularly their scale free size and duration distributions, reveals information regarding the system that are nearly universal in nature, i.e., they depend on only a few parameters such as the interaction range in such systems, their dimensions, and so on [1–3]. The properties of avalanches are also used in hazard assessments of certain systems, where such assessments are crucial. For example, it is well established that the size distributions of avalanches if sampled near a catastrophic failure point, show an exponent value that is smaller than what one would obtain if all avalanches are sampled [4]. Specifically, in shear dynamics of compressed granular media, the avalanche size distribution exponent is known to depend on the differential stress [5]. The same is observed in earthquake statistics, i.e., the Guttenberg-Richter exponent changes in the regions where larger events are likely to occur [6,7]. There are other ways to extract meaningful information from the avalanche statistics near the breaking point, for example the inequality of avalanches shows universal precursors that signal imminent breakdown [8,9].

In this work, we study the evolution of a breaking process for a disordered system that is driven towards catastrophic breakdown. Particularly, we use the fiber bundle model, which is a paradigmatic model for fracture of disordered solids [2]. It is a threshold activated model, where a collection of elements of different load carrying capacities carries an overall external load. When the external load is applied gradually, the system goes through intermittent avalanches of breaking events that eventually culminate, for a sufficiently high external load, at a global failure. The individual avalanches that take the system from one stable state to the other (until global failure) have multiple steps of stress field readjustments within them. For example, if S number of fibers break in an avalanche, that breaking happens through several subavalanches, such that the sum of all subavalanche sizes within an avalanche equals the size of that avalanche. The sizes of the subavalanches are the numbers of fibers broken in one step of load redistribution, and the number of load redistribution steps is denoted by the duration τ of the avalanche.

The temporal shapes of avalanches in the fiber bundle model have been looked at before in different contexts [10,11], particularly for a creep rupture, i.e., a constant load and external noise and also with load induced failures in different dimensions. It was found that, for a given duration of an avalanche, the shapes become more symmetric as the dimensionality increases. As we shall discuss later on, this is consistent with our observations here, but looks at a different limit than what we report here.

The temporal shape of an avalanche has been investigated in other avalanching systems also, both theoretically and experimentally [12–16]. Particularly, when an "elastic" interface is driven through a disordered medium, it goes through stick-slip motions, showing avalanches. With a "slow" (compared to the avalanche duration) drive and associated dissipation (acoustic and other such forms of energy emissions), dynamics of such driven interfaces reach a self-organized critical

*Contact author: soumyajyoti.b@srmap.edu.in
†Contact author: psphy@caluniv.ac.in

(SOC) state. Among other things, one property of an SOC system is that the critical point is an attractive fixed point and the SOC systems always reside close to it. With this being said, the temporal shapes of the avalanches were shown to depend on the nature of "elasticity" of the driven interface. Particularly, it was shown [12] that for sufficiently local range of the interaction kernel in the driven interface the time-reversal symmetry of the avalanches is broken, while for sufficiently nonlocal kernels the shapes are symmetric under time reversal. In the mean field limit, therefore, the direction of time cannot be determined by looking at the time variations of the stress field readjustments within an ongoing avalanche (or similar other manifestations of the dynamics). However, these assertions (dependence of time-reversal asymmetry on nonlocality of interaction kernels) are studied only close to the critical point. A more generic approach to modeling avalanche was by various forms of (returning) random walks [17]. It was shown [18] that such avalanche shapes follow universal features for uncorrelated stochastic processes, while for correlated processes the shapes of avalanches could become asymmetric. The effect of dimensionality, particularly near the upper critical dimensions, was also studied for the avalanche shapes [19].

Here we look at the variations of the avalanche shapes in disordered systems, starting far away from the critical point and gradually approaching the breakdown point. We find that the avalanche shapes are asymmetric away from the critical point and become symmetric as the critical point is approached, even for a mean field interaction. Given that the system is mean field, the symmetry at the critical point is expected. For the same reason, therefore, a reduction of asymmetry could be a useful indicator of the approaching criticality. We show that there is a universal trend in approaching a time-reversal symmetric avalanche pattern in the fiber bundle model of fracture with quasistatic load increase that does not depend on the type of disorder present in the model. We also study other modes of load increase, viz., the load increase by a discrete amount. The dynamical class of the system is known to be different under this loading condition. Here, we solve analytically the dynamics of the model. The analytical solution of the dynamical equations show that the avalanche shapes under this loading condition is always asymmetric. The full functional form could be obtained in this case.

II. THE MODEL AND ITS AVALANCHE DYNAMICS

The fiber bundle model is a threshold activated model for fracture of disordered solids that can capture many qualitative features of fracture dynamics, for example the intermittent scale-free avalanche statistics. In this study of the evolution of a fiber bundle with time, we consider L fibers arranged in parallel. These fibers carry an external mechanical load. The fibers are assumed to be linear elastic elements which can bear load up to a threshold σ_{th}. After reaching the threshold capacity, the fibers break irreversibly. The values of these thresholds for the individual fibers are randomly sampled from a probability density function $\rho(\sigma_{\text{th}})$. Unless otherwise specified, this function is uniform in the domain (0,1) [20].

To initiate the dynamics of the failure process, an initial load σ_0 is applied on each fiber. The fibers with threshold $\sigma_{\text{th}} > \sigma_0$ will survive and the remaining fibers will break irreversibly. The load applied on the failed fibers is redistributed equally to all the surviving fibers. Because of this increase in the load of the surviving fibers, further fibers may break. The process of redistribution will continues until no more fibers break, i.e., all thresholds are higher than the applied load per fiber value or the entire system has broken down. In the former case, the load is increased again.

It is important to clarify the notations used here at this point. The number of fibers broken between two successive load increase is called an avalanche S, while the number of fibers breaking in each step of redistribution is called a subavalanche s. We denote by t' the time step of load redistribution within an avalanche (t' runs from 0 to τ for an avalanche of duration τ). Here t' simply counts the redistribution steps. On the other hand, we denote by t the total time elapsed since the start of load application on the intact system. This means, at the start of the nth avalanche, $t = \sum_{i=1}^{n-1} \tau_i$ and t' has run from 0 to τ_i for all i between 1 to n.

There are two kinds of loading protocols that we will deal with here. These are distinguished based on how the load is increased once the system reaches a stable configuration. One protocol is to increase the load uniformly on all surviving fibers by an amount $\delta\sigma$ that is the minimum required value in order to break the fiber which is closest to its breaking point i.e., $\delta\sigma = \min(\sigma_{\text{th}}^i - \sigma_i)\ \forall\, i$, where σ_i denotes load on the ith intact fiber. This process will restart the dynamics by breaking exactly one fiber (the one closest to the failure threshold) and the avalanche may continue. This is called the quasistatic loading protocol. In the other protocol, the increment of load is always by a constant amount to the system (note that increment of load per fiber will progressively increase, since the number of surviving fibers decreases). This is called the discrete loading protocol. The avalanche initiation step here will typically cause more than one fiber to break, and the dynamics may continue thereafter. These two types of loading protocols are profoundly different in terms of the corresponding avalanche statistics. Particularly, while both protocols produce scale-free size distributions for the avalanches, the exponent values differ; it is $-5/2$ in the former [21] (Eq. (208) of [2]) and -3 in the latter [22] (Eq. (139) of [2]).

In this work, we study the avalanche shapes for both these loading protocols under mean field and localized load sharing and study the time-reversal symmetry of the avalanche shapes and its universal properties near the breaking point.

III. AVERAGE AVALANCHE SHAPE IN THE CASE OF QUASISTATIC LOADING

As mentioned above, with quasistatic loading, the avalanche of fiber failures [14] starts with a single fiber failing (the one closest to failure), causing the load to be redistributed onto the remaining intact fibers, which can lead to further breaking events. $S(\tau)$ denotes the size of an avalanche having a duration τ. Its magnitude, of course, is the sum of its constituent subavalanches $s_\tau(t')$:

$$S = \sum_{t'=0}^{\tau} s_\tau(t'), \tag{1}$$

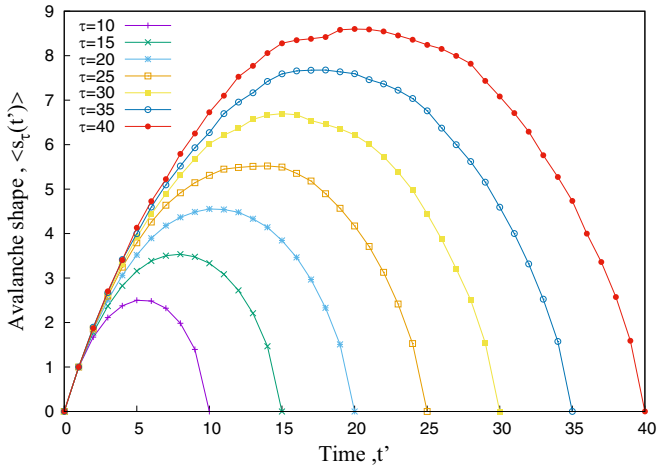

FIG. 1. The shape of an avalanche is shown as the time (step of load redistribution) variation of subavalanche sizes. The average avalanche shapes $\langle s_\tau(t')\rangle$ for different specific durations (τ) of the avalanches are shown from simulations for uniform threshold distribution under quasistatic loading, system size $L = 100\,000$, and number of samples is 10 000.

where the index t' refers to an integer value that tracks the number of redistribution steps, as mentioned before. The stress field relaxation process within the system (i.e., the load redistribution steps) is assumed to be much faster than the external load increase rate (hence the quasistatic nature of loading). Therefore, the total load can be taken as constant during an ongoing avalanche process. This makes it possible to consider the duration of an avalanche τ to be a proxy for the total load on the system; i.e., the duration is, on average, a monotonically increasing function of the total load on the system, as a reflection of the diverging timescale with the proximity to the failure point. To calculate the asymmetry of the avalanches we define the average shape as follows: we generate an ensemble of N samples having the same failure threshold distribution. Let $\overline{s_\tau^{(\alpha)}(t')}$ ($t' = 1$ to τ) denote the average value of $s_\tau(t')$ obtained from all avalanches of a particular duration τ in the α-th sample. The ensemble average of this quantity is defined as the average shape given by

$$\langle s_\tau(t')\rangle = \frac{1}{N}\sum_{\alpha=1}^{N}\overline{s_\tau^{(\alpha)}(t')}. \tag{2}$$

The data for the average shape as a function of t' are plotted after rescaling the x axis by the duration τ (making it vary between 0 to 1) and the y axis by the maximum height of the avalanche shape profile (making it vary between 0 to 1 also), shown in Fig. 1. This process was repeated for different types of threshold distributions: uniform, Gaussian, and triangular, each within the range (0,1) (see Fig. 2). Then, the asymmetry of the resulting average avalanche profile (denoted by $\langle s_{t'}\rangle$) is calculated from [23]

$$A = \frac{1}{\langle s_{\max}\rangle\tau}\sum_{t'=0}^{\tau}|\langle s_\tau(t')\rangle - \min\{\langle s_\tau(t')\rangle, \langle s_\tau(\tau - t')\rangle\}|. \tag{3}$$

Defined in this way, a fully (time-reversal) symmetric shape would give $A = 0$. As can be seen in Fig. 3, a plot of the above mentioned asymmetry measure with the corresponding average initiating load (load per fiber at the time when an avalanche was started) shows a sharp decrease as the critical load (σ_c, the load per fiber value at which the system collapses) is approached [see Fig. 3(a)]. This form of the decrease is found to be universal, i.e., it does not depend on the particular threshold distribution used [see Fig. 3(b)]. Indeed, an approximate power-law fitting suggests

$$A \sim (\sigma_c - \sigma)^{1/4} \tag{4}$$

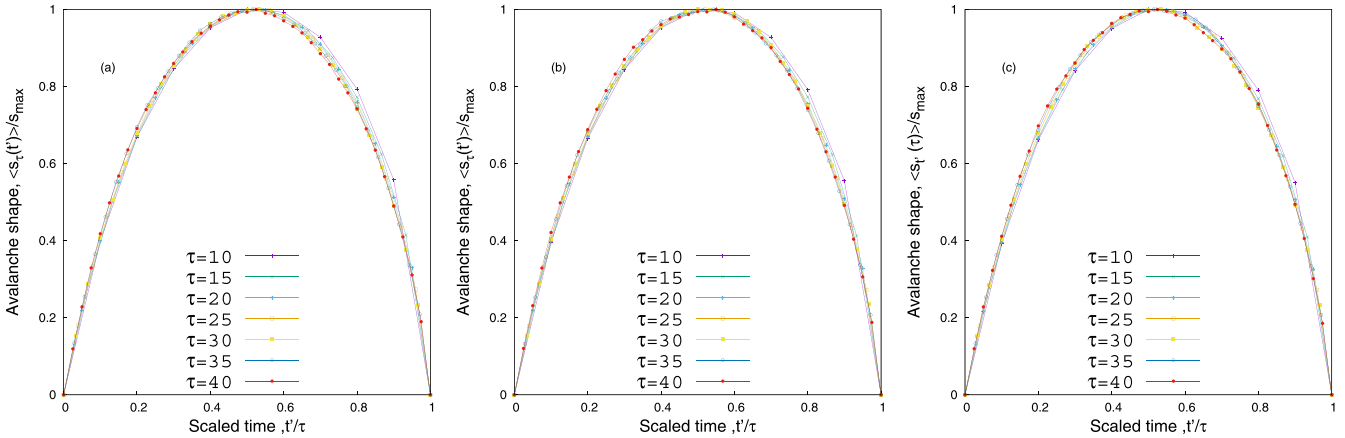

FIG. 2. Average avalanche shapes for avalanches with of duration τ for various disorder disorder distribution functions. (a) Uniform distribution, (b) triangular distribution, (c) Gaussian distribution. The load redistribution steps t' are scaled by the avalanche duration τ and the subavalanche sizes (number of fibers breaking in one load redistribution) are scaled by the maximum value for each duration. While generally the shape is that of an inverted parabola, there are deviations from this symmetric shape, as the the system approaches failure (higher avalanche duration here is a proxy to higher applied load, which in turn indicates imminent failure). For simulations, system size is $L = 50\,000$ and number of samples is 30 000.

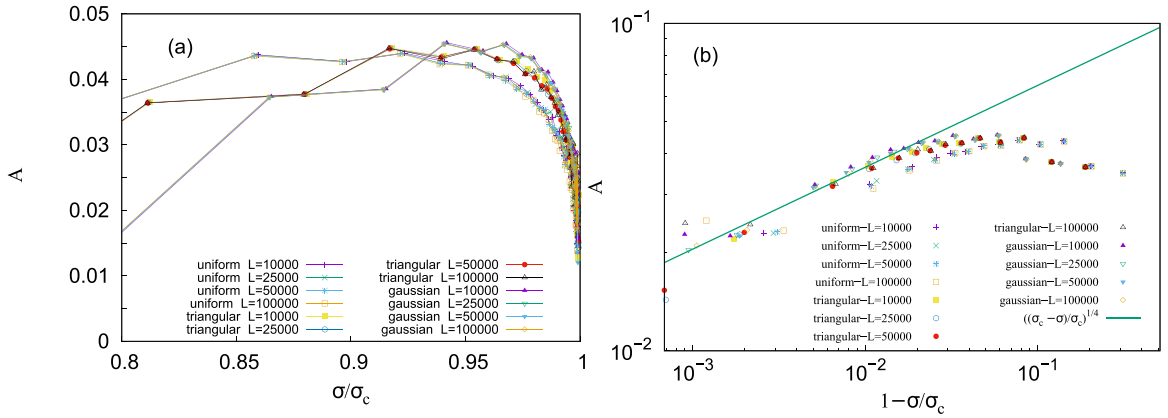

FIG. 3. Plot showing the variation of the asymmetry of the avalanches [measured using Eq. (3)] with the scaled external load on the system for which the avalanche of a particular duration had started. The larger duration avalanches start with a higher load. The initial small-sized avalanches are symmetric, but the avalanches become more asymmetric from higher loads. However, as the system nears the failure point, the avalanches start becoming more symmetric, which is then an indication of imminent failure. For simulations, the number of samples used varied between 20 000 to 100 000 for the largest ($L = 100\,000$) to the smallest ($L = 20\,000$) system sizes.

for all three types of threshold distributions [see Fig. 3(b)]. These results also do not seem to have any systematic system size dependence.

It is interesting to note here the size distribution of the avalanches of a particular duration (see Fig. 4). While the size distribution of all avalanches is expected to be a power-law (with exponent value $-5/2$), when looked at for a specific duration, the size distributions are no longer scale free. Indeed, the scale of the avalanche sizes (for example, the average or the most probable value) increases monotonically with duration. This is expected for the correspondence between avalanches of longer duration and that of the average initiating load on the system. A fit of the most probable values show a power-law of exponent -1.25. This non-scale-free structure of the individual components of an overall scale-free distribution has a resemblance to similar observations in wealth distribution models [24].

IV. SOLUTIONS TO THE DYNAMICAL PROCESS IN DISCRETE LOADING

Now we consider the case when the load is increased by a fixed amount in each step. The breaking dynamics [the evolution of $U(t)$, the surviving fraction of fibers at time t] can be solved analytically for this case of discrete loading. While such solutions have been looked at previously for the case when the system is very close to the breaking point, here we attempt a solution for the entire range of the dynamics and thereby get a form for the avalanche shapes under this loading protocol.

To do that, we consider the initial threshold distribution to be uniform within the range (0,1). Then, for any subsequent step of the dynamics, the threshold distribution of the remaining part of the system will be a uniform distribution within the domain $(\sigma_L, \sigma_R = 1)$. This is because, as soon as a fixed load is applied, the weaker fibers will break, i.e., the weaker part of the distribution will disappear, resulting in a gradual increase in the values of σ_L. Indeed, the values of σ_L will be a function of $U(t)$, the surviving fraction of fibers at time t, with the understanding that only the strongest fibers survive, i.e., $U(t)$ is also the fraction of the strongest fibers of the initial sample. This simplification is a result of the mean field nature of the dynamics and does not apply to any localized load distribution process where there is stress concentration around damaged regions.

In what follows, we first solve $U(t)$ for fixed values of σ_L and σ_R when a load σ_0 is applied. For this case, of course, in the beginning $\sigma_L = 0$ and $\sigma_0 = \delta$. Each loading step will then give a time evolution of $U(t)$. As we shall see, this is a transcendental equation and needs to be evaluated numerically. The saturation value of $U(t) = U^*$, for each loading step, gives the surviving fraction of fibers in that step. Using that we get the updated value of $\sigma_L = \sigma_0/U^*$. Then we follow the time evolution again, when the load is increased to $\sigma_0/U^* + \delta$, with the updated value of σ_L, and so on. In this way, the entire time evolution of the surviving fraction could be obtained.

The cumulative distribution of the thresholds [20] can be written as

$$P(\sigma_{\rm th}) = \begin{cases} 0, & \sigma_{\rm th} < \sigma_L, \\ \dfrac{\sigma_{\rm th} - \sigma_L}{\sigma_R - \sigma_L}, & \sigma_L \leqslant \sigma_{\rm th} \leqslant \sigma_R, \\ 1, & \sigma_{\rm th} \geqslant \sigma_R. \end{cases} \tag{5}$$

For the above mentioned threshold distribution of the stress values, the recursive relation of the failure process [20] is written as

$$U_{t+1} = \frac{1}{\sigma_R - \sigma_L}\left(\sigma_R - \frac{\sigma_o}{U_t}\right), \tag{6}$$

which can be converted to a differential equation (in the limit of continuous t, or in this case large L) of the form

$$\frac{dU}{dt} = \frac{1}{\sigma_R - \sigma_L}\frac{\sigma_R U - \sigma_0 - U^2(\sigma_R - \sigma_L)}{U}. \tag{7}$$

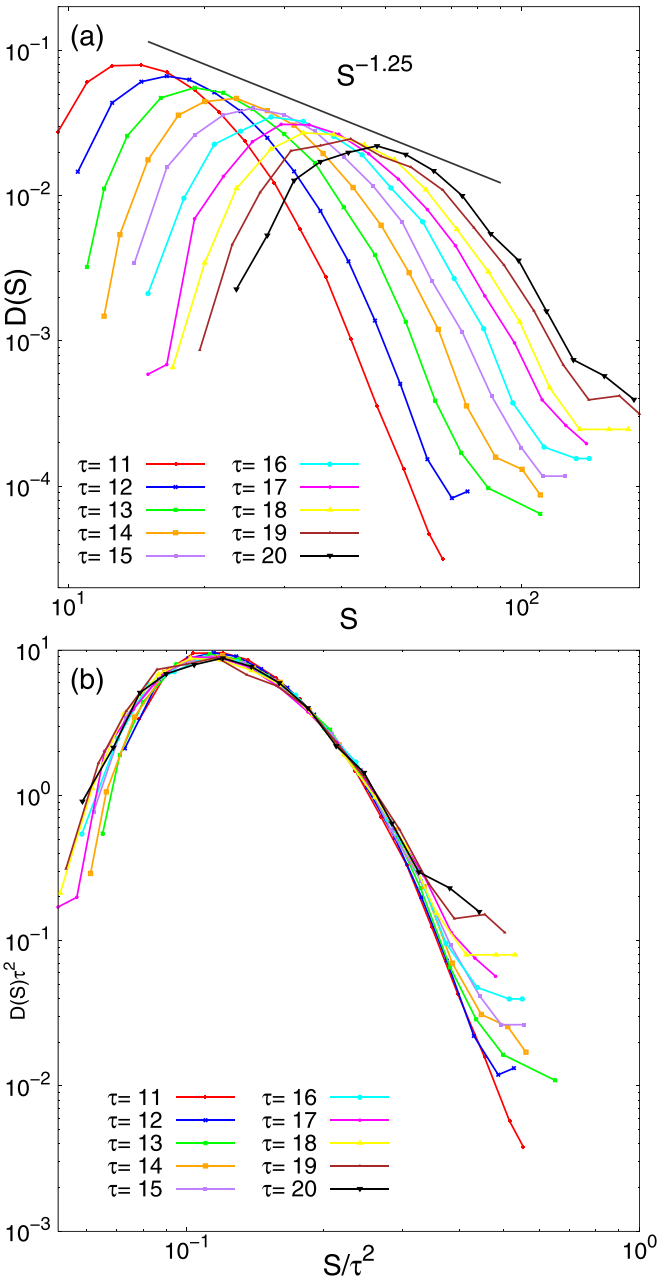

FIG. 4. (a) Probability distribution $D(S)$ of avalanche size S for uniform threshold distributions for different specific durations (τ) of avalanche (with increasing values of τ from left to right). (b) Collapsed data of the probability of the avalanche size for different specific durations of the avalanche τ. For the simulations, system size is $L = 100\,000$ and number of samples is 10 000.

Using the partial fraction method, the above equation can be solved as

$$-t = \frac{1}{2}\int \frac{2U(\sigma_R-\sigma_L)-\sigma_R}{U^2(\sigma_R-\sigma_L)-\sigma_R U+\sigma_o}dU + \frac{1}{2}\int \frac{\sigma_R}{U^2(\sigma_R-\sigma_L)-\sigma_R U+\sigma_o}dU. \quad (8)$$

Now setting $b = \frac{\sigma_R}{\sigma_R-\sigma_L}$, $c = \frac{\sigma_o}{\sigma_R-\sigma_L}$, the transformed equation after solving will give us the evolution of the surviving fraction of fibers $U(t)$ when the system is applied with an initial load per fiber σ_o:

$$-t = \frac{1}{2}\ln|U^2(\sigma_R-\sigma_L)-\sigma_R U+\sigma_0| + \frac{b}{4\sqrt{\frac{b^2}{4}-c}}\ln\left|\frac{2U-b-2\sqrt{\frac{b^2}{4}-c}}{2U-b+2\sqrt{\frac{b^2}{4}-c}}\right| + \ln k \quad (9)$$

where

$$\ln k = -\frac{1}{2}\ln|(\sigma_R-\sigma_L)-\sigma_R+\sigma_0| - \frac{b}{4\sqrt{\frac{b^2}{4}-c}}\ln\left|\frac{2-b-2\sqrt{\frac{b^2}{4}-c}}{2-b+2\sqrt{\frac{b^2}{4}-c}}\right|.$$

While a closed form solution of the above equation for $U(t)$ is not possible, the dynamics of the model follow this equation for the entire range of time evolution. This is a general case of the special condition where such dynamics were solved [20] only near the stable points, leading to an evaluation of the relaxation time scale.

However, here we are interested in the temporal shape of the avalanches, which can be obtained numerically from the above equation.

A. Numerical calculation and simulations of failure process in ELS model

Equation (9) gives the time evolution of the fraction of surviving fibers in the model when the failure thresholds of the individual fibers are distributed uniformly within (σ_L, σ_R) and an initial load σ_0 is applied on the intact system.

The numerical solution of Eq. (9) is done by decreasing U from 1 iterative by a small amount (0.00001) until the corresponding value of t increases. The point beyond which t starts decreasing [as obtained from Eq. (9)] is the solution for that combination of $\sigma_0, \sigma_L, \sigma_R$. The validity of this process can be checked in Fig. 5, where comparisons with numerical simulations for $L = 100\,000$ are made for different values of σ_0. The saturation limit of $U(t)$ is the stable limit of the surviving fraction, generally denoted as U^*, corresponding to the applied load σ_0.

Our aim, of course, is to solve the dynamics for successive load increments on the system. The basic scheme for that is to rescale σ_L, σ_0, and U at the beginning of each loading step. The dynamical equation is the same and the same solution process described above is applied, except with the rescaled values of the parameters. This is possible only in the mean-field limit, where the fibers break strictly in the same order as their individual failure thresholds (hence, effectively σ_L increases). The rescalings are done as follows: σ_0 is adjusted to increase such that it takes the value $\sigma_0/U^* + \delta$, σ_L is adjusted to the value σ_0/U^*, U is set at 1. After solving Eq. (9) and finding the corresponding U^*, it is multiplied with the U^* of the previous step. This process is repeated successively, for each loading step. An additional input was also used: As can be seen from Fig. 5, the time at which the surviving fraction of fibers reach saturation in the simulation is earlier than what is seen from the numerical evaluation of Eq. (9). This is because,

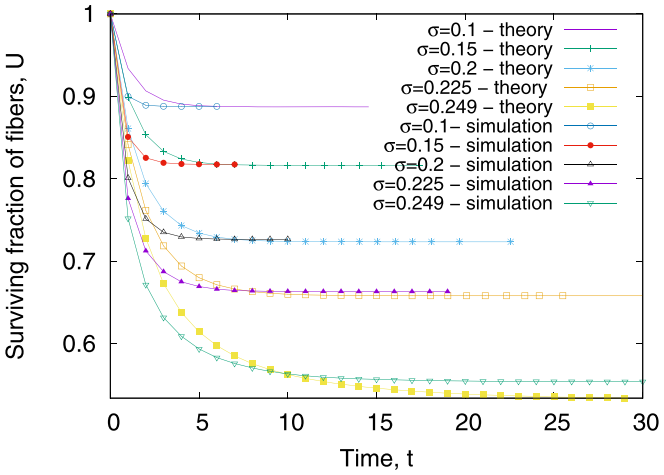

FIG. 5. The theoretical estimates [numerically solving Eq. (9)] and the simulation results of the surviving fraction of fibers $U(t, \sigma_0)$ as a function of redistribution (time) steps, when the system is loaded with several values of initial load per fiber σ_0, with initial condition $U(t = 0, \sigma_0) = 1$ in each case. The saturation value of surviving fraction decreases as the initial load increases. The threshold distributions are uniform in (0,1) and the system size $L = 100\,000$ for the simulations.

numerically, U can change by an arbitrarily small amount, but in simulations the change is bounded from below by $1/L$. Therefore, we keep saturation time from the simulations, while evaluating U^* numerically from Eq. (9). The resulting variation of the fraction of surviving fibers is shown in Fig. 6, along with the corresponding numerical solution. They match satisfactorily.

Now, the avalanche shape can be obtained just by differentiating $U(t)$. Clearly, the saturation values of $U(t)$ give

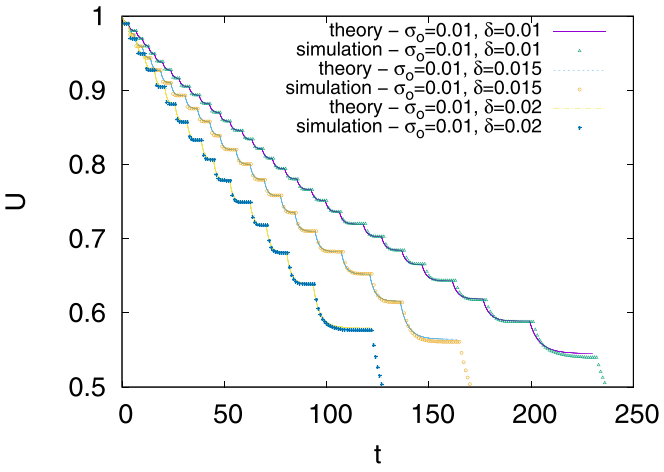

FIG. 6. The comparison between the theoretical [from numerical solution of Eq. (9)] and simulation results for the surviving fraction of fibers as the load is increased in equal steps every time the surviving fraction reaches saturation. The saturation time limit for the surviving fraction is taken as an input from the simulation while evaluating the theoretical curves. The saturation values for the surviving fractions match very well between the simulations and the theoretical estimates. The initial threshold distribution is uniform in (0,1) and the system size for simulations is $L = 100\,000$.

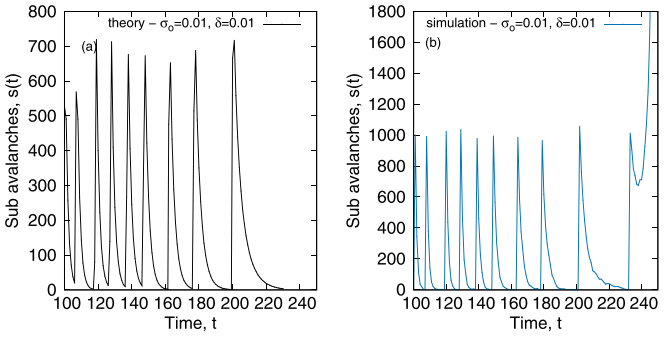

FIG. 7. Theoretical (a) and simulation (b) (as in Fig. 6) results of the recursive dynamics for the avalanche size with system size ($L = 100\,000$ fibers). Theoretical curves are obtained by differentiation of data of Fig. 6. The area between two successive zeros of the function gives one avalanche of size S.

zero when differentiated. Such zeros segregate the avalanches from each other. The avalanche shapes, obtained from the numerical evaluation and simulations, are shown in Fig. 7. Although the widths (i.e., duration) of the avalanches match, the maximum heights are different, again as the approach to saturation value depends on numerical choice of integration steps for U. Nevertheless, the asymmetry in the shapes of the avalanches remains unchanged and consistent during the entire dynamical process.

The codes used for these steps are made available in the Supplemental Material [25].

B. Avalanche shape prior to catastrophic failure with variable load redistribution range

Here, we look at the shape of the avalanches when the load sharing is local. Particularly, we look at the case where the load of a broken fiber is shared between R nearest surviving neighbors (in a one-dimensional lattice). The loading protocol is the discrete load increase. The system size used is $L = 50\,000$.

While taking the averages of the simulation results, we record the subavalanche sizes of the last three avalanches that occur just before the catastrophic event. This is because the manifestation of symmetry, if any, will be most prominent just prior to the critical point. We then calculated the average shape of these three avalanches to understand the pattern before the breakdown took place. The avalanche shapes are always asymmetric in this case, as seen from Fig. 8.

V. DISCUSSIONS AND CONCLUSIONS

The intermittent avalanche dynamics in driven disordered systems show remarkable statistical regularities. Particularly, the size distributions of avalanches are known to follow power-law distributions, with exponent values that are only dependent on the ranges of interactions and dimensionality of the system, and do not depend on the other system specific details, such as the distributions of disorders within the system, and so on. Such regularities have been studied in great detail both theoretically and experimentally. However, much less is known about the time variation profile of the individual avalanches.

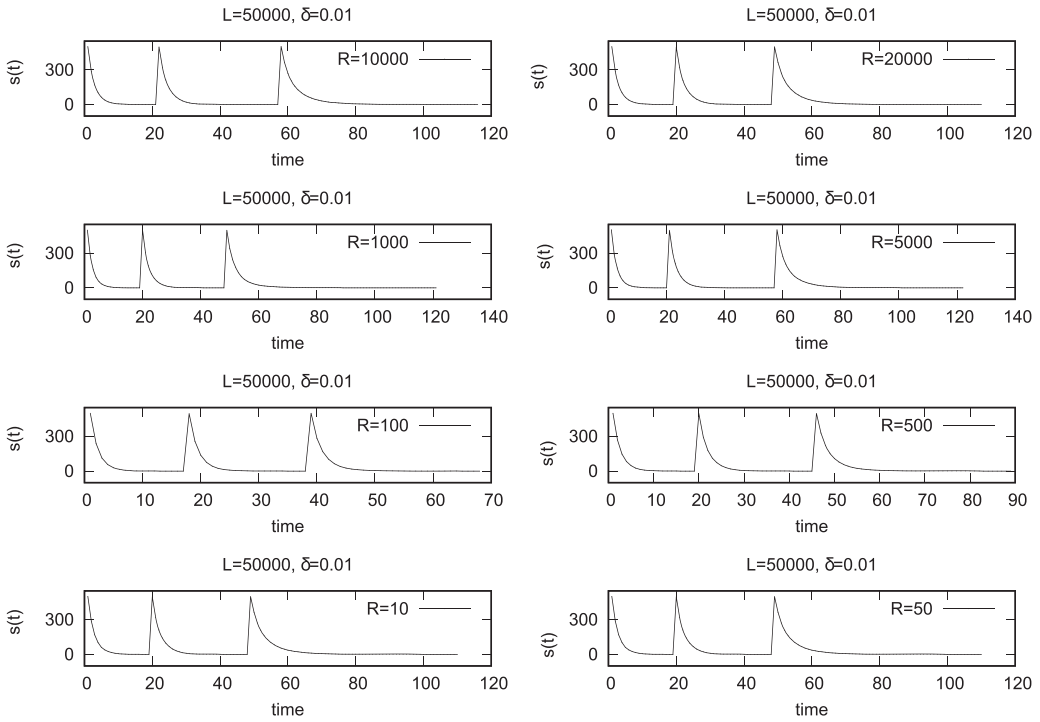

FIG. 8. Simulation results showing last three avalanches before the catastrophic event under discrete loading; load redistribution is varied by different interaction ranges R. The avalanche shape remains asymmetric irrespective of the value of R.

Here we looked at this question of temporal avalanche shapes in the fiber bundle model of fracture, primarily in the mean-field limit. While it is known that near the critical point the avalanche shapes, for mean-field systems, are symmetric with respect to time reversal, here we have shown that away from the critical point, under quasistatic loading protocol, the symmetry is broken. Therefore, quantification of asymmetry for the avalanches leads to a drastic drop as the system approaches the failure point (see Fig. 3). The functional form [see Eq. (4)] of the variation of the asymmetry in the avalanche shapes is universal, in the sense that it does not depend upon the threshold distributions of the fibers. Also, there is no systematic system size dependence. Therefore, monitoring the shapes of avalanches could serve as a useful indicator of the imminent failure. It is important to note here that in Ref. [11] the avalanche shapes in fiber bundles of higher dimensions show that, for a fixed duration, the shape becomes more symmetric with increase in dimensions. Their quantification of asymmetry also shows that, with duration, the asymmetry decreases for high dimensions (mean-field limit), which is consistent with what we note here. But here we also show the functional form of the variation of asymmetry as the failure point is approached, which could not be concluded from Ref. [11].

We also study the avalanche shapes for the discrete loading protocol. While the dynamical evolution of the avalanche shapes is partially analytically tractable in this case, the shapes are always asymmetric, both in the mean field and local load sharing limit.

In conclusion, the temporal shapes of avalanche for the fiber bundle model under quasistatic loading tend from an asymmetric to symmetric shape, in a universal manner, as the catastrophic breakdown point is approached.

ACKNOWLEDGMENTS

The numerical simulations are performed in HPCC Surya at SRM University–AP. P.S. acknowledges financial support from the SERB Project (DST, Govt. of India) No. MTR/2020/000356.

[1] S. Biswas, P. Ray, and B. K. Chakrabarti, *Statistical Physics of Fracture, Breakdown, and Earthquake: Effects of Disorder and Heterogeneity* (John Wiley & Sons, New York, 2015).

[2] S. Pradhan, A. Hansen, and B. K. Chakrabarti, Failure processes in elastic fiber bundles, Rev. Mod. Phys. **82**, 499 (2010).

[3] M. J. Alava, P. K. Nukala, and S. Zapperi, Statistical models of fracture, Adv. Phys. **55**, 349 (2006).

[4] C. Scholz, The frequency-magnitude relation of microfracturing in rock and its relation to earthquakes, Bull. Seismol. Soc. Am. **58**, 399 (1968).

[5] T. Hatano, C. Narteau, and P. Shebalin, Common dependence on stress for the statistics of granular avalanches and earthquakes, Sci. Rep. **5**, 12280 (2015).

[6] D. Schorlemmer, S. Wiemer, and M. Wyss, Variations in earthquake-size distribution across different stress regimes, Nature (London) **437**, 539 (2005).

[7] C. Narteau, S. Byrdina, P. Shebalin, and D. Schorlemmer, Common dependence on stress for the two fundamental laws of statistical seismology, Nature (London) **462**, 642 (2009).

[8] Diksha and S. Biswas, Prediction of imminent failure using supervised learning in a fiber bundle model, Phys. Rev. E **106**, 025003 (2022).
[9] Diksha, S. Kundu, B. K. Chakrabarti, and S. Biswas, Inequality of avalanche sizes in models of fracture, Phys. Rev. E **108**, 014103 (2023).
[10] Z. Danku and F. Kun, Temporal and spacial evolution of bursts in creep rupture, Phys. Rev. Lett. **111**, 084302 (2013).
[11] Z. Danku, G. Ódor, and F. Kun, Avalanche dynamics in higher-dimensional fiber bundle models, Phys. Rev. E **98**, 042126 (2018).
[12] L. Laurson, X. Illa, S. Santucci, K. Tore Tallakstad, K. J. Måløy, and M. J. Alava, Evolution of the average avalanche shape with the universality class, Nat. Commun. **4**, 2927 (2013).
[13] J. P. Gleeson and R. Durrett, Temporal profiles of avalanches on networks, Nat. Commun. **8**, 1227 (2017).
[14] A. Batool, Z. Danku, G. Pál, and F. Kun, Temporal evolution of failure avalanches of the fiber bundle model on complex networks, Chaos **32**, 063121 (2022).
[15] S. Papanikolaou, F. Bohn, R. L. Sommer, G. Durin, S. Zapperi, and J. P. Sethna, Universality beyond power laws and the average avalanche shape, Nat. Phys. **7**, 316 (2011).
[16] S. Zapperi, C. Castellano, F. Colaiori, and G. Durin, Signature of effective mass in crackling-noise asymmetry, Nat. Phys. **1**, 46 (2005).
[17] A. Baldassarri, F. Colaiori, and C. Castellano, Average shape of a fluctuation: Universality in excursions of stochastic processes, Phys. Rev. Lett. **90**, 060601 (2003).
[18] F. Colaiori, A. Baldassarri, and C. Castellano, Average trajectory of returning walks, Phys. Rev. E **69**, 041105 (2004).
[19] A. Dobrinevski, P. Le Doussal, and K. J. Wiese, Avalanche shape and exponents beyond mean-field theory, Europhys. Lett. **108**, 66002 (2014).
[20] P. Bhattacharyya, S. Pradhan, and B. K. Chakrabarti, Phase transition in fiber bundle models with recursive dynamics, Phys. Rev. E **67**, 046122 (2003).
[21] P. C. Hemmer and A. Hansen, The distribution of simultaneous fiber failures in fiber bundles, J. Appl. Mech. **59**, 909 (1992).
[22] S. Pradhan, P. Bhattacharyya, and B. K. Chakrabarti, Dynamic critical behavior of failure and plastic deformation in the random fiber bundle model, Phys. Rev. E **66**, 016116 (2002).
[23] N. Hohmann and E. Jarochowska, Enforced symmetry: The necessity of symmetric waxing and waning, PeerJ **7**, e8011 (2019).
[24] M. Patriarca, A. Chakraborti, and G. Germano, Influence of saving propensity on the power-law tail of the wealth distribution, Physica A **369**, 723 (2006).
[25] See Supplemental Material at http://link.aps.org/supplemental/10.1103/PhysRevE.110.014129 for the codes used in this paper.